STK4 deficiency underlies impaired interferon signaling and T cell immunity

Andrea Guennoun
Sidra Medicine
Salim Bougarn
Sidra Medicine
Taushif Khan
Sidra Medicine
Rafah Mackeh
Sidra Medicine
Mahbuba Rahman
Sidra Medicine
Fatima Al Ali
Sidra Medicine
Manar Ata
Sidra Medicine
Waleed Aamer
Sidra Medicine
Debra Prosser
Sidra Medicine
Tanwir Habib
Sidra Medicine
Evonne Chin-Smith
Sidra Medicine
Khawla Al-Darwish
Sidra Medicine
Qian Zhang
The Rockefeller University
Alya Al-Shakaki
Weill Cornell Medicine-Qatar
Amal Robay
Weill Cornell Medicine-Qatar
Ronald Crystal
Weill Cornell Medicine
Khalid Fakhro

Sidra Medicine
Amal Al-Naimi
Sidra Medicine
Eman Al Maslamani
Sidra Medicine
Amjad Tuffaha
Sidra Medicine
Ibrahim Janahi
Sidra Medicine
Mohammad Janahi
Sidra Medicine
Donald Love
Sidra Medicine
Mohammed Yousuf Karim
Sidra Medicine
Bernice Lo
Sidra Medicine
Amel Hassan
Sidra Medicine
Mehdi Adeli
Sidra Medicine
Nico Marr (nmarr@sidra.org)
Sidra Medicine https://orcid.org/0000-0002-1927-7072

Research Article

Keywords: Human serine/threonine kinase 4 (STK4) deficiency, combined immunodeficiency, T cell lymphopenia, interferon, antibody repertoire, transcriptomics

Posted Date: March 22nd, 2021

DOI: https://doi.org/10.21203/rs.3.rs-328827/v1

STK4 deficiency underlies impaired interferon signaling and T cell immunity

Andrea Guennoun[§,1], Salim Bougarn[§,1], Taushif Khan[1], Rafah Mackeh[1], Mahbuba Rahman, Fatima Al-Ali[1], Manar Ata[1], Waleed Aamer[1], Debra Prosser, Tanwir Habib, Evonne Chin-Smith[1], Khawla Al-Darwish, Qian Zhang[3], Alya Al-Shakaki[4], Amal Robay[4], Ronald Crystal[5], Khalid Fakhro[1,4,6], Amal Al-Naimi[7], Eman Al Maslamani[7], Amjad Tuffaha, Ibrahim Janahi[7], Mohammad Janahi[7], Donald R. Love[ψ,2], Mohammed Yousuf Karim[ψ2], Bernice Lo[ψ1,6], Amel Hassan[ψ,7], Mehdi Adeli[ψ,7], Nico Marr[1,6] (ORCID: 0000-0002-1927-7072)

1 Research Branch, Sidra Medicine, Doha, Qatar

2 Department of Pathology, Sidra Medicine, Doha, Qatar

3 St. Giles Laboratory of Human Genetics of Infectious Diseases, Rockefeller Branch, The Rockefeller University, New York, NY, USA

4 Weill Cornell Medicine-Qatar, Doha, Qatar

5 Weill Cornell Medicine, New York, USA

6 College of Health and Life Sciences, Hamad bin Khalifa University, Doha, Qatar

7 Department of Pediatrics, Sidra Medicine, Doha, Qatar

§, ψ, equal contribution

Address correspondence to: Nico Marr, Sidra Medicine, Research Branch, Doha, Qatar, PO BOX 26999, E-mail: nmarr@sidra.org

Abstract

Purpose. Human serine/threonine kinase 4 (STK4) deficiency is a rare, autosomal recessive genetic disorder leading to combined immunodeficiency. The extent to which STK4 deficiency impairs immune signaling and host defenses is unclear. We assessed the functional consequences of a novel, homozygous nonsense STK4 mutation (NM_006282.2:c.871C>T, p.Arg291*) found in a pediatric patient by comparing the patient's innate and adaptive cell-mediated and humoral immune responses with those of three heterozygous relatives and unrelated controls.

Methods. The genetic etiology was identified by whole genome sequencing and confirmed by Sanger sequencing. STK4 gene and protein expression was measured by quantitative RT-PCR and immunoblotting, respectively. Cellular abnormalities were assessed by high-throughput RT-RCR, RNA-Seq, ELISA and polychromatic flow cytometry. Finally, antibody responses were delinated by ELISA and phage immunoprecipitation-sequencing.

Results. The affected patient exhibited partial loss of STK4 expression and complete loss of STK4 function. The patient suffered from recurrent viral and bacterial infections, most notably persistent Epstein-Barr virus viremia and pulmonary tuberculosis. Cellular and molecular analyses revealed abnormalities to the fractions of T-cell subsets, plasmacytoid dendritic cells, and NK cells. The transcriptional responses of the patient's whole blood and PBMC samples were reminiscent of dysregulated interferon signaling, impaired T immunity and increased T-cell apoptosis. Nonetheless, the patient had detectable vaccine-specific antibodies and IgG responses to various pathogens, consistent with a normal CD19+ B-cell fraction, albeit with a distinctive antibody repertoire, largely driven by herpesvirus antigens.

Conclusion. Patients with STK4 deficiency can exhibit broad impairment of immune function extending beyond lymphoid cells.

Keywords

Human serine/threonine kinase 4 (STK4) deficiency; combined immunodeficiency; T cell lymphopenia; interferon; antibody repertoire; transcriptomics

Introduction

Human serine/threonine kinase 4 (STK4) deficiency is a rare autosomal recessive (AR) genetic disorder leading to a combined immunodeficiency with severe T cell lymphopenia. This condition is characterized by a predisposition to a wide range of bacterial and viral infectious diseases, mucocutaneous candidiasis, lymphomas and congenital heart disease (1). To date, STK4 deficiency has been reported in relatively few patients. Therefore, the extent to which immune signaling and host defense mechanisms are impaired or dysregulated in affected individuals remains incompletely understood. However, the spectrum of clinical manifestations associated with STK4 deficiency has been steadily increasing with each new case report.

STK4 deficiency was first reported by Nehme *et al.* in two patients from unrelated Turkish families harboring a homozygous nonsense mutation in the *STK4* gene (2). The patients experienced complications due to recurrent bacterial and viral infections, most notably persistent Epstein–Barr virus (EBV) viremia, which ultimately resulted in Hodgkin B cell lymphoma. Due to weak expression of the homing receptors CCR7 and CD62L, the authors attributed the underlying mechanism of STK4 deficiency to increased death of naïve and proliferating T cells, and impaired homing of $CD8^+$ T cells to secondary lymphoid organs (2). Abdollahpour *et al.* reported the cases of three siblings of Iranian descent with a homozygous premature stop codon in the *STK4* gene (3). These patients suffered from T and B cell lymphopenia, intermittent neutropenia, and atrial septal defects, as well as recurrent bacterial and viral infections, mucocutaneous candidiasis, cutaneous warts, and skin abscesses. Interestingly, Schipp *et al.* reported a Turkish patient with STK4 deficiency who developed a highly malignant B cell lymphoma at the age of 10 years and a second, independent Hodgkin lymphoma 5 years later. However, no detectable EBV or other common virus infection was detected in this patient. The authors speculated that the lymphoma may have developed due to the lack of the tumor suppressive function of STK4, or perturbed immune surveillance due to the diminished $CD4^+$ T cell compartment (4). In contrast, most malignancies reported in

patients with STK4 deficiency are associated with prolonged EBV viremia, ultimately leading to the development of B cell lymphomas (2, 5-7). More specifically, patients present with Hodgkin B cell lymphoma (2), extranodal marginal zone lymphoma of mucosa-associated lymphoid tissue (8), Burkitt's lymphoma (7), or maxillary sinus diffuse large B-cell lymphoma (9). Additional clinical features in patients with STK4 deficiency include salt-losing tubulopathy, suggestive of an acquired Gitelman syndrome, immune complex glomerulonephritis, and Castleman-like disease (10), juvenile idiopathic arthritis (11), human betapapillomavirus-associated epidermodysplasia verruciformis (11, 12) and primary cardiac T cell lymphoma (6).

Studies in mice and humans have shown that STK4 plays a pivotal role in lymphocyte function by regulating integrin-dependent T lymphocyte trafficking, proliferation and differentiation (13, 14). Of note, the STK4 protein is broadly expressed in various human haemopoietic cells, most notably monocytes, and is not restricted to lymphocytes (https://www.proteinatlas.org/ENSG00000101109-STK4). However, its role in T cell-independent functions is less well understood. Recently, Jørgensen *et al.* studied innate immune signaling in the context of STK4 deficiency by *in vitro* stimulation or infection of PBMCs obtained from an 11-year-old female $STK4^{-/-}$ patient of a consanguineous Syrian family. These studies revealed defective type I/II and III interferon (IFN) responses to a variety of purified Toll-like receptor (TLR) agonists, live viruses or bacterial lysates due to impaired phosphorylation of the kinase TBK1 and the transcription factor IRF3 (15). The results also revealed increased apoptosis in STK4-deficient T cells and neutrophil granulocytes, as well as a decreased FoxO3a expression in STK4-deficient T cells, further supporting the important role of STK4 in T cell survival.

In this study, we identified an AR STK4 deficiency in a child from consanguineous parents, which was due to a novel homozygous stop-gain mutation in a region encoding a coiled-coil domain located downstream of the kinase domain. We investigated the functional consequences of the new variant on innate and adaptive cell-mediated, as well as humoral

111 immune responses.

112

Methods

Whole-genome sequencing

Genomic DNA (gDNA) was isolated from the peripheral blood of the subjects using DNeasy® Blood & Tissue Kits (Qiagen LLC, Germantown, MD, USA) according to the manufacturer's instructions. Whole genome sequences were obtained using a standard library preparation protocol and an Illumina HiSeq-X platform to generate 150-bp paired-end sequences. The raw sequencing reads were mapped to the reference genome (GRCh37, hg19) using BWA (version 0.7.15) (16), and genetic variants were called with the HaplotypeCaller in the GATK suite (v.4.0) (17). The Variant Call Format (VCF) file, containing variants, was annotated using SnpEff v.4.3 (18) and filtered for the candidate fitting the following criteria: (1) Being in the coding region including the exonic, splice-site region, (2) being rare (<1%) in all mutation databases (i.e., 1,000 genomes, gnomAD, ExAC, and ESP6500), and (3) co-segregates with the phenotype in the family and follows a specific mode of inheritance (for example, AR). The final list of variants was prioritized based on the literature search and whether any of the associated genes had been linked to the patient's symptoms, such as known Mendelian genes (https://omim.org).

Sanger sequencing. Primers seq_STK4_Ex8F (5'-GTCCGAAGCACAAAGAGAAAGA-3') and seq_STK4_Ex8R (5'-CCAGCTCCAAGTTGATCCAATA-3') were designed to flank exon 8 of the STK4 gene (NM_006282.5; LRG_535t1), checked for underlying single nucleotide polymorphisms, and synthesized as described previously (19). The forward and reverse primers were tailed with M13 sequences: CACGACGTTGTAAAACGAC (added to the 5' end of the forward primer), and CAGGAAACAGCTATGACC (added to the 5' end of the reverse primer). DNA was extracted from peripheral blood using a QIAsymphony® SP and QIAsymphony DSP DNA Midi Kit (Qiagen Pty Ltd). DNA quantity and quality were assessed using a NanoDrop® ND-1000 spectrophotometer (Thermo Scientific, Wilmington, DE, USA). Genomic DNA (50ng) was subjected to conventional PCR using the following conditions: 95°C

for 10 minutes, then 34 cycles of 95°C for 30 seconds, 60°C for 30 seconds and 72°C for 45 seconds, with a final incubation at 72°C for 5 minutes. Amplicons were checked for correct size and non-specific amplification prior to ExoSAP-IT cleanup, cycle sequencing using primers comprising the M13 tails, and BigDyeXTerminator cleanup followed by loading onto an Applied Biosystems model 3500XL Genetic Analyzer. Sequence data were analyzed using Applied Biosystems Sequence Analysis software, and Mutation Surveyor software.

RT-qPCR analysis of STK4 gene expression levels. For *STK4* gene expression analysis, PBMCs were isolated from the patient, parents and healthy donors by Ficoll-gradient centrifugation. Cells were then incubated with T cell activation and expansion beads (anti-CD2/CD3/CD28; Miltenyi Biotec, Gaithersburg, MD, USA) for 10 days in 5% CO_2 at 37°C. On day 3, the medium was supplemented with IL-2 (100 U/ml) to promote cell proliferation. RNA was extracted from 1 million cells using TRIzol lysis reagent (Thermo Fisher Scientific, Carlsbad, CA, USA) according to the manufacturer's instructions**.** Briefly, 1 million cells were lysed in 1ml of TRIzol for 3 minutes, then 140 μl of chloroform were added, and the phases were separated by centrifugation at 4°C and 16000 x *g*. RNA-containing liquid phase was mixed to an equal volume of isopropanol and the mixture was incubated for 10 minutes at room temperature for RNA precipitation. After centrifugation, precipitated RNAs were de-salted by incubation with 1/10 volume of 5 M NH4OAc and 2.5 volumes of 100% cold ethanol, followed by washing with 75% ethanol and final elution in nuclease free water. The *STK4* transcript was quantified using Fast SYBR Green Master Mix (Applied Biosciences) with the following primers: forward 5'-TGGAGACGGTACAGCTGAGG-3'; reverse 5'-ATAGCAACAATCTGGCCGGT-3'. All reactions were performed in triplicate using a QuantStudio 6K Flex real-time PCR System (Applied Biosciences). Data were normalized to the expression of the housekeeping gene *RPLP0* (Ribosomal protein, large, P0) and mean ΔCt^{-1} values were plotted.

Western blot analysis. T cells were derived from PBMCs as described above and T cell lysates (containing 20 μg total protein) were separated using 4%–15% tris-glycine Bis-Tris Gels (BioRad). Following electrophoresis, proteins were transferred to a polyvinylidene fluoride (PVDF) membrane. After blocking with 5% non-fat milk in tris-buffered saline (TBS) for 1 h, the membrane was incubated overnight at 4°C in TBS in the presence of anti-recombinant STK4 antibody (diluted 1:5,000) (Abcam, clone EP1465Y, catalog no. ab51134), α-tubulin monoclonal antibody (diluted 1:10,000) (Cell Signaling Technology, Denvers, MA, USA, catalog no. 3873), or anti-β-actin antibody (diluted 1:5,000) (Santa-Cruz Biotechnology, Dallas, TX, USA, catalog no. sc-47778). Membranes were then washed (3 x 5 min) with TBS with 0.1% Tween-20 (TBS-T) and then incubated in TBS with a 1:5,000 dilution of either horse-radish peroxidase (HRP)-conjugated goat anti-rabbit (Invitrogen, Frederick, MD, USA, catalog no. 65-6120), or goat anti-mouse (Invitrogen, Frederick, MD, USA, catalog no. 31430) secondary antibody, for 1 h at room temperature. Membranes were washed again (3 x 5 min) in TBS-T. Immunoreactive proteins were visualized using enhanced chemiluminescence (ECL™) (Amersham) according to the manufacturer's instructions. Images were acquired on ChemiDoc MP imaging system (BioRad).

In vitro stimulation of whole blood and high-throughput gene expression analysis. Peripheral blood was collected into sodium heparin vacutainer tubes. After incubation for 2 h at room temperature, 2 ml WB was diluted with an equal amount of RPMI 1640 media containing GlutaMax™ (Gibco). The samples were then stimulated for 2 h at 37°C with the following agonists (final concentrations are shown): ultrapure LPS of *E. coli* K12 (InvivoGen) at 10 ng/ml; R848 (InvivoGen) at 3 μg/ml; Poly(I:C) (high molecular weight) (InvivoGen) at 25 μg/ml; recombinant human IL-1β (R&D Systems) at 20 ng/ml; a 1:1 mix of recombinant human IFN-α2 and IFN-β (R&D Systems) at 1,000 IU/ml each; recombinant human IFN-γ (R&D Systems) at 1,000 IU/ml; recombinant human TNF-α (R&D Systems) at 20 ng/ml; 5'ppp-dsRNA/LyoVec™ (InvivoGen) at 1 μg/ml; Poly(dA:dT)/LyoVec™ (InvivoGen) at 10 ng/ml; 3'3'-

cGAMP/LyoVec™ (InvivoGen) at 10 µg/ml; MDP (InvivoGen) at 10 ng/ml; Dynabeads™ Human T-Activator CD3/CD28 (Invitrogen) at 400,000 beads/ml; AffiniPure F(ab')$_2$ fragment goat anti-human IgG + IgM (H+L) (Jackson ImmunoResearch) at 10 µg/ml; or PMA/ionomycin calcium salt (Sigma) at 40 ng/ml and 1µg/ml. Similarly, cells were incubated for 2 h at 37°C with LyoVec™ alone or RPMI media as unstimulated control samples. Subsequently, three volumes of Tempus™ solution (Applied Biosystems) were added for cell lysis and RNA stabilization before total RNA was isolated using the Tempus™ Spin RNA isolation kit (Applied Biosystems). RNA quality and quantity were assessed using an Agilent 2100 Bioanalyzer (Agilent Technologies) and NanoDrop 1000 (Thermo Fisher Scientific). The cDNA of all 180 target genes and six housekeeping genes was generated from 40 ng total RNA using a reverse transcription master mix (Fluidigm) and quantified using custom Delta Gene™ assays in combination with 96.96 Dynamic Array™ IFCs and the BioMark™ HD microfluidic system (Fluidigm) in accordance with the manufacturer's instructions. All 180 target genes and six housekeeping genes (**Supplemental Table S3**) were selected *a priori* from a larger set of 1,088 transcripts, represented by 66 sets of co-expressed genes (transcriptional modules), which had previously been found to be responsive in WB stimulation with purified PRR agonists, recombinant cytokines and pyogenic bacteria (20). We selected three representative genes per transcriptional module for a total of 60 modules based on their closeness to the median absolute expression of all transcripts assigned to a given module. Six modules were excluded from the analysis due to limited functional annotation. Housekeeping genes were selected from the same dataset (GSE25742) as previously described (21). Expression levels of the 180 target genes were quantified relative to the six housekeeping genes using the $2^{-\Delta\Delta Ct}$ method (22). We evaluated fold changes in expression as $\log_2$-transformed expression level (log2FC) for each target gene under each stimulation condition and filtered for genes with a $|\text{log2FC}| \geq 1$ in at least two samples. Next, we computed z-score values of the log2FC for each gene and condition in the patient using two unrelated control subjects and the three heterozygous family members as controls. Finally, we used principal component analysis to estimate the variance in z-scores across samples. The first two principal components

described approximately 75% of the variance in the z-score profile of samples and a distinct segregation of patient and control subjects was observed (**Supplemental Figure S3**). We extracted the contribution factor for each gene from the PCA and filtered for pairs of target gene and stimulation condition that showed a variance of |log2FC| >1 between the patient and control subjects, resulting in the identification of 28 target genes that were differentially expressed under one or more (*i.e.* up to eight) *in vitro* stimulation conditions (**Figure 4 and Supplemental Table S3**).

PBMC stimulation and RNA-Seq analysis. Peripheral blood was collected into sodium heparin vacutainer tubes, PBMCs were isolated by Ficoll-Paque (GE Healthcare) density gradient centrifugation according to the manufacturer's instructions and frozen in fetal bovine serum containing 20% dimethyl sulfoxide. For *in vitro* stimulation, PBMCs where thawed, rested for 24 h and then stimulated with a 1:1 mix of recombinant human IFN-α2 and IFN-β (R&D Systems), PMA/ionomycin, or left unstimulated as described for the stimulation of whole blood samples. Total RNA was isolated using the RNeasy Mini Kit (QIAGEN) according to the manufacturer's instructions. RNA integrity and purity were evaluated using a Bioanalyzer 2100 (Agilent Technologies Genomics). cDNA was generated using the SMARTer v4 Ultra® Low Input RNA for Sequencing Kit (Takara Bio). Resulting cDNA was quantified and size-controlled using a Bioanalyzer 2100 (Agilent Technologies Genomics). cDNA was normalized to 1 ng/μl and libraries were prepared using the Nextera XT DNA Library Preparation Kit (Illumina) and the Nextera XT Index Kit v2 set A (Illumina), respectively, in accordance with the manufacturer's instructions. 150 bp paired-end sequencing to approximately 20 million reads per sample was performed using a HiSeq4000 system (Illumina). Raw reads were aligned to the UCSC human genome assembly version hg38 using STAR aligner (23). The HTSeq-count (24) tool was used to count the number of reads that mapped to each gene feature. Read counts were adjusted to mitigate batch effects by negative binomial regression models using comBat-Seq (25). After read counts were normalized, we removed genes expressed at low

levels using the HTSFilter and the default protocol. We finally calculated log2FC values for each subject and stimulation condition relative to the unstimulated condition of the same subject using edgeR (26). Genes with a |log2FC| ≥1 were considered differentially expressed. Residual responses were calculated as described previously (27). Gene enrichment analysis was performed using the QIAGEN IPA software application.

Phage immunoprecipitation-sequencing (PhIP-Seq). The VirScan phage library used for PhIP-Seq in the present study was obtained from S. Elledge (Brigham and Women's Hospital and Harvard Medical School, Boston, MA, USA). PhIP-Seq was performed as described previously (28-30) using an expanded version of the original VirScan phage library (31). We computed species-specific adjusted score values as described earlier (30, 32). Pooled human plasma used for IVIg (Privigen® CSL Behring AG) and human IgG-depleted serum (Molecular Innovations, Inc.) served as additional controls.

Flow cytometry. Lymphocyte subsets were assessed using Duraclone assays (Beckman Coulter) to delineate major lymphocyte subsets (IM Phenotyping Basic) and more specifically, T cell and dendritic cell subsets (IM T cell and IM DCs) according to the manufacturer's protocol. Samples were analyzed with a FACSymphony A5 Flow Cytometer (BD Biosciences) and FlowJo 10.5.2 software.

Absolute blood cell counts, total immunoglobulin levels, vaccine-specific antibody measurements and QuantiFERON-TB Gold ELISA

Complete blood cell and lymphocyte counts, total immunoglobulin measurements (i.e., IgG, IgA, IgM), vaccine-specific antibody measurements (i.e., anti-diphtheria toxoid IgG, anti-*Haemophilus influenzae* Type B, anti-pneumococcus capsular poly Ab, anti-tetanus toxoid antibody) and whole blood IFN-γ measurements in response to Mtb peptide antigens (QuantiFERON-TB Gold ELISA, QIAGEN, Germantown, MD, USA) were carried out and interpreted by laboratories accredited by the College of American Pathologists (CAP) following

277 the manufacturer's instructions and clinical guidelines. Normal ranges were provided in tables
278 and figures as appropriate. An "indeterminate" test result of the QuantiFERON-TB Gold ELISA
279 indicated the patient's lymphocytes also did not respond to mitogen stimulation (can be seen
280 in immunodeficiency, lymphopenia, overwhelming infection, malnutrition, and with
281 immunosuppressive medications).
282
283 ***Statistical analysis.*** For PhIP-Seq experiments, we imputed -$\log_{10}$(*P*-values) by fitting a zero-
284 inflated generalized Poisson model to the distribution of output counts followed by regression
285 of the parameters for each peptide sequence based on the input read count. Peptides that
286 passed a reproducibility threshold of -$\log_{10}$(*P*-value) $\geq$2.3 in two technical sample replicates
287 were considered significantly enriched.
288

Results

Clinical description of the case and family members. The patient was the third child of consanguineous parents (first-degree cousins). The patient had a younger sibling who was healthy, as were both parents. Of note, the parents reported the death of the two elder siblings of the patient. One died with a history of chronic headache, coughing and lymphoma, while the other died with a history of chronic coughing (**Figure 1A**). However, no detailed medical records or genetic data were available for the two deceased siblings.

The patient suffered from recurrent skin rashes starting from infancy, recurrent chest infections since early childhood, and an overall failure to thrive with low weight gain and short stature (data not shown). The patient's early medical history included a productive cough of yellow/white mucoid sputum associated with on/off fever, which was more common at bedtime; however, early medical records were very limited and likely to be incomplete. The patient was more closely followed clinically starting at elementary school age. He was diagnosed with bronchiectasis and asthma, and started on asthma control medication, including Ventolin. He also experienced complications due to recurrent viral and bacterial infections, chronic suppurative otitis media and recurrent pneumonia. The patient was also diagnosed with tuberculosis (TB), which was confirmed by *Mycobacteria tuberculosis* complex positive culture, while a QuantiFERON assay, performed in parallel, had an "indeterminate" test result (see methods for details). The patient was subsequently treated for pulmonary TB for approximately one year. After being off treatment for another year, the patient suffered from TB reactivation, and was again put on anti-TB medication (cycloserine, linezolid, moxifloxacin and pyrazinamide) for two years. He also presented with a lower chest infection as a teenager and a chest X-ray confirmed lower left consolidation. A sputum culture revealed heavy growth of *Haemophilus influenzae* and *Streptococcus pneumoniae*, as well as light growth of methicillin-resistant *Staphylococcus aureus*. About a year later, the patient was hospitalized again with a second episode of lower chest infection by *H. influenzae* and multiple-drug resistant *Klebsiella*

316 *pneumoniae*. EBV viremia was detected during early teenage years, and repeated testing
317 confirmed persistent EBV viremia up to the most recent follow-up. During the teenage years,
318 he also suffered from intermittent neutropenia and severe lymphopenia (**Supplemental**
319 **Figures S1A, S1B and S1C)** with markedly decreased naïve $CD45RA^+$ cells (11.1%; normal
320 range: 46%–77%); the onset may have been earlier but was not detected due to the late
321 diagnosis. Antibody responses to childhood vaccination were within the normal range
322 (**Supplemental Table S1**).
323
324 ***Homozygosity for a stop-gain mutation in the STK4 gene.*** We performed whole genome
325 sequencing on the patient and all of his immediate family members, except the deceased
326 sisters. The analysis revealed a rare, homozygous nonsense mutation in the *STK4* gene
327 (NM_006282.2:c.871C>T, p.Arg291*) in the patient, whereas both parents and the younger
328 sibling were identified as heterozygous carriers, suggesting an AR inheritance pattern (**Figure**
329 **1A**). The *STK4* genotypes of the patient and his family members were confirmed by clinical
330 Sanger sequencing (**Figure 1B**). The combined annotation-dependent depletion (CADD)
331 score of the variant was 42, providing further evidence of its deleteriousness (**Figure 1C and**
332 **D**).
333
334 ***The mutant STK4 allele is a loss-of-function (LOF) variant.*** The mutant STK4 protein was
335 not detected in PBMC-derived T cells from the patient by Western blot analysis using a
336 monoclonal antibody directed against the N-terminus of the protein, whereas intermediary
337 levels of the STK4 protein were found in the parents compared to two unrelated healthy
338 controls (**Figure 1E**). We also assessed the impact of the *STK4* variant at the transcript level.
339 A *STK4* transcript was detectable in PBMC-derived T cells of the patient, albeit at reduced
340 levels compared to controls with a wild-type genotype and the heterozygous parents
341 (**Supplemental Figure S2A and B**).
342

Reduced fractions of naïve T helper, and dendritic cell subsets, as well as increased effector memory and apoptotic T helper and precursor NK cells in the PBMCs of the patient. We performed polychromatic flow cytometric analyses of PBMCs obtained from the patient at middle-school-age in order to compare the lymphocyte subset distribution with that of his parents, his younger sibling and one unrelated control **(Figure 2**)**.** As expected, we found a lower fraction of T cells in the patient compared to the controls (**Figure 2A, B and C**), which was mainly attributed to selective $CD4^+$ T cell lymphopenia (**Figure 2C**). The $CD19^+$ B cell population was not affected in the patient (11.7%) when compared to the controls (range 10.9%–20.8 %) (**Figure 2A**). Similarly, $CD56^+CD3^-$ NK cells of the patient (4.59%) were within the normal range compared to the control subjects (range 1.87%–6.82%) (**Figure 2B**). However, we noticed a significant increase of the $CD56^{bright}$ NK cell subset in the patient (1.78%) compared to all controls (range 0.058%–0.42%) (**Figure 2B**). We then assessed $CD4^+$ T cell subsets and found an increase in programmed death-1 (PD-1)-expressing T helper cells in the patient (**Figure 2D**). Next, we analyzed PBMCs expression of CD45RA and CCR7 and detected low frequencies of $CD45RA^+CCR7^+$ double-positive naïve T cells in the patient, while his $CD45RA^-CCR7^-$ effector memory population was increased (**Figure 2E**). Similarly, the $CD27^+CD28^+$ T cell subset, which consists mainly of naïve T cells, was also slightly decreased in the patient (**Figure 2F**). Finally, assessment of the dendritic cell (DC) subsets showed a decrease of $CD11c^-CD123^+$ plasmacytoid DCs (pDCs) in the patient, while his $CD11c^+CD123^-$ myeloid DCs (mDCs) population remained normal (**Figure 2E**).

The patient has a distinct antiviral antibody repertoire. To further assess the humoral immunity status of the patient, we performed large-scale antibody profiling by phage immunoprecipitation-sequencing (PhIP-Seq) using serum samples obtained from the patient. We found the patient to be seropositive for antibodies specific to a variety of common viruses and bacteria, including human herpesviruses (HHV)-4 (EBV), -5 (CMV) and -8, enterovirus (EV)-B, and human respiratory syncytial virus (HRSV), human rhinoviruses (HRV) A and B, *S. pneumoniae* and *S. aureus* (**Figure 3A**). The antibody repertoire breadth in the patient was

similar to that of the controls (**Figure 3B**). Nevertheless, principal component analysis of the enriched antibody-antigen interactions showed an overall distinct antibody repertoire in the patient compared to those of his family members and unrelated controls (**Figure 3C**), which was largely driven by antibodies targeting HHV-4 and -5 antigens (**Figure 3D**).

Gene expression signatures suggest dysregulated interferon signaling and impaired T cell activation, inhibition of T cell proliferation and increased T cell apoptosis. To further elucidate the functional consequences of STK4 deficiency at the molecular level, we performed gene expression analyses using either whole blood (WB) samples or PBMCs isolated from the patient and control subjects following *in vitro* stimulation with a variety of immune activators. First, we stimulated WB of the patient, his family members and an unrelated control subject with purified pattern recognition receptor (PRR) agonists [lipopolysaccharides of *E. coli* K12 (LPS_{K12}) (a TLR4 agonist), muramyl dipeptide (MDP) (a NOD2 agonist), Poly(I:C) (a TLR3 agonist), Poly(dA:dT) (a multiple-PRR agonist), resiquimod (R848) (a TLR7/8 agonist), cyclic guanosine monophosphate-adenosine monophosphate (cGAMP) (a STING agonist), and 5' triphosphate double-stranded RNA (5'ppp-dsRNA) (a RIG-I agonist)], cytokines [IFN-α/IFN-β (an interferon-α/β receptor IFNAR agonist), IFN-γ, IL-1β and TNF-α], a potent mitogen [phorbol 12-myristate 13-acetate (PMA)/ionomycin] and BCR or TCR activators. We measured the expression of 180 functionally well-annotated target genes, which we had selected *a priori* from a larger set of genes responsive to WB stimulation with purified PRR agonists, recombinant cytokines and pyogenic bacteria (20) (see methods and **Supplemental Table S3** for further details); mock stimulations served as controls. We then filtered for differentially expressed genes (DEGs) among the 180 target genes for which the transcriptional responses in the patient's WB samples to any of the *in vitro* stimulation conditions showed high variance in comparison to those of the other family members and the unrelated control (**Supplemental Figure S3**). The identified DEGs were associated with caspases and apoptosis, type I and II interferon signaling, inflammation, cell signaling, and

ubiquitination, as well as cell movement and phagocytosis (**Figure 4** and **Supplemental Table S4**).

Finally, we performed mRNA-Seq of PBMCs isolated from the patient and following stimulation with PMA/ionomycin, IFN-α/IFN-β, or unstimulated. Both parents and three unrelated, healthy controls were assessed for comparison. We filtered for DEGs in response to each stimulation condition and found a profound dysregulation of IFN-regulated gene expression, although IFN-induced gene expression was not completely abrogated (**Figure 5A**). We then performed a gene enrichment analysis on the identified DEGs using the QIAGEN Ingenuity Pathway Analysis (IPA) software application. We focused our downstream analysis on canonical pathways that were differentially activated or inhibited in the patient's cells, compared to those of the controls. In response to IFNAR activation, nine pathways were differentially regulated in the patient compared to the controls, most of which are linked to T cell signaling and apoptosis, cell proliferation, oxidative stress and interestingly, IL-23 signaling (**Figure 5B**). Similarly, we observed several pathways that are normally repressed following mitogen activation, but instead were highly activated or dysregulated in the patient's cells. These included pathways primarily involved in T cell effector functions, T and B cell activation, cell cycle arrest and apoptosis (**Figure 5B**). Given the apparent dysregulation of IL-23 signaling in the patient's cells, we also examined absolute *IL-23* and *IFNG* gene expression, either at baseline, or following stimulation with PMA/ionomycin. We found that in comparison to the control subjects, *IL-23* gene expression in the patient was highly impaired at baseline and largely unresponsive to PMA/ionomycin stimulation, whereas *IFNG* gene expression appeared normal (**Supplemental Figure S3C and D**).

Discussion

Due to the relatively small number of patients reported to date, the extent to which immune signaling and host defense mechanisms are impaired or dysregulated in patients with STK4 deficiency remains incompletely understood. Here, we describe a male pediatric patient with AR complete STK4 deficiency and a clinical history of recurrent viral and bacterial infections, persistent EBV viremia and pulmonary TB. The underlying stop-gain mutation was found to be located in a genomic region that encodes the coiled-coil domain of STK4, downstream of its protein kinase domain. We were unable to detect even a truncated STK4 protein in the patient using a monoclonal antibody to the N-terminal region of STK4, suggesting that protein expression of the mutated allele is completely abrogated due to nonsense-mediated decay.

In accordance with earlier case reports (5, 8, 33), we found that the PBMCs isolated from the patient in this study had reduced fractions of $CD4^+$ naïve but increased effector memory T helper cell subsets compared with those in the $STK4^{wt/mut}$ family members and an unrelated $STK4^{wt/wt}$ control. Furthermore, flow cytometric analysis showed a considerable proportion of the remaining T helper cell subset in the patient expressed higher levels of PD-1, and our RNA-Seq analyses revealed dysregulation of several pathways in the patient, suggesting elevated T cell exhaustion and impaired effector functions of the residual T cells. Whether this is a consequence of persistent EBV viremia (34-36) or an intrinsic feature of STK4 deficiency, or perhaps both, remains to be established. Previous studies have shown that EBV reactivation correlates with the expression of PD-1/PD-L1 antigens in patients with proliferative glomerulonephritis (37). On the other hand, $CD4^+$ T cell lymphopenia has also been reported in STK4-deficient patients in the absence of detectable EBV infection (4). In addition, the patient presented with episodes of intermittent neutropenia, which is consistent with previous observations (2, 3, 6, 9).

Our results also highlight that STK4 deficiency can lead to the impairment of a variety of T cell-independent and innate immune responses. Indeed, we detected a considerable proportion of $CD56^{bright}$ NK cells in the PBMCs isolated from the patient. While these cells constitute only a small fraction of NK cells in the peripheral blood in healthy individuals, they represent the majority of NK cells in secondary lymphoid tissues. $CD56^{bright}$ NK cells are thought to be the precursors of NK cells (38) and may have immunoregulatory properties (39). We also observed a decreased fraction of pDCs in the patient's peripheral blood. Whether this is an indirect consequence of active EBV infection, as shown in mouse studies (40), or whether low levels of pDCs contribute directly to a lack of EBV control, remains unclear. In accordance with the recent findings reported by Jørgensen *et al.* (15), we observed dysregulated type I and II IFN signaling in the patient's cells. Interestingly, transcriptomic analysis of the patient's PBMCs in response to IFNAR activation *in vitro* revealed a profound dysregulation of IFN-regulated gene expression, affecting interferon-stimulated genes (ISGs) that are primarily associated with T cell activation and proliferation, although IFN-induced gene expression was not completely abrogated. This suggests that suboptimal IFN signaling may contribute to the T cell immunodeficiency and the vulnerability of STK4-deficient patients to viral infection and cancer development. However, overall fractions of $CD19^{+}$ B cells (**Figure 2A**) and IgG antibody responses to childhood vaccination (**Supplemental Table S1**) or common microbial infection (**Figure 3**) did not appear to be diminished in our patient, apart from our observation that antibody specificities were largely targeting HHV-4 and -5 antigens. Of note, a recent study in $STK4^{-/-}$ mice and nine patients from five unrelated families with STK4 deficiency has suggested that STK4 is required for normal humoral immunity, since KO mice and patients had reduced marginal zone B (MZB) cells, as well as reduced numbers of innate-like B-1b cell subsets, while the overall fractions of circulating $CD19^{+}$ B cells were normal as in our patient (41). This raises the question whether patients with STK4 deficiency may also be selectively impaired to mount robust T cell-independent, polysaccharide-specific antibody responses to control natural infection with encapsulated bacteria, such as *H. influenzae, K. pneumoniae* and *S. pneumoniae*, which would be consistent with the clinical history of our patient.

Polysaccharide-specific antibody responses (or the lack thereof) would have been undetectable by the PhIP-Seq assay performed in this study, as it exclusively detects antibodies that target protein antigens and has limitations for the detection of conformational as well as post-translationally modified epitopes (28). High efficacy of plain polysaccharide-based vaccines also depends on the maturation of MZB cells, which usually does not occur until the second year of life (42). In our patient, the specific antibody responses were at the lower end of our laboratory reference range (**Supplemental Table S1**). However, anti-pneumococcal polysaccharide antibodies cannot necessarily be utilized as markers of MZB cell-mediated immunity, due to the introduction of the conjugate pneumococcal vaccine into the local routine immunization schedule. The literature shows variability for specific antibody responses in STK4-deficient patients, ranging from normal to absent (41). The infection history of our patient with *H. influenzae, K. pneumoniae* and *S. pneumoniae* could have also interfered with the utility and interpretation of vaccine response tests using plain polysaccharide vaccines. Therefore, humoral immunity of patients with STK4 deficiency towards encapsulated bacteria requires further investigation.

We also demonstrated a profound impairment of *IL-23* gene expression in the patient's PBMCs, both at baseline and following *in vitro* stimulation. IL-23 is produced by innate lymphoid cells, gamma-delta T cells, DCs and macrophages, and it has been shown that *IL-23*-dependent IFN-γ immunity plays a pivotal role in controlling *Mycobacterium tuberculosis* (Mtb) infection (43). It is therefore tempting to speculate that impaired *IL-23* gene expression may have contributed to the susceptibility of the patient to pulmonary TB, confirmed on sputum culture. Despite the clinical evidence of pulmonary TB, the patient's QuantiFERON test result was indeterminate, i.e., the patient's lymphocytes did not respond to mitogen stimulation. This is likely to reflect a combination of the cellular dysfunction and profound lymphopenia. Of note, Radwan *et al.* (7) also speculated that complications in a 9-year-old Egyptian boy with STK4 deficiency were associated with mycobacterial infection, albeit tuberculin skin-test results were

negative and the results from QuantiFERON tests were also inconclusive in this Egyptian patient.

It remains unclear whether malignancies in STK4-deficient patients are a secondary consequence of persistent EBV viremia, or whether patients with STK4 deficiency are inherently prone to malignancies due to dysregulation of oncogenes even in the absence of EBV infection (4). Interestingly, our RNA-Seq experiments revealed upregulation of mitogen-induced B cell-activating factor (BAFF) receptor gene (*TNFRSF13C*) expression in the patient, suggesting activation of BAFF signaling, in contrast to the controls where this pathway was inhibited following PMA/ionomycin stimulation (**Figure 5 and Supplemental Table S2**). Studies *in vitro* and in mice have shown that EBV drives autonomous B cell proliferation (44), which also depends on T cell-independent survival signals provided by the BAFF receptor. Excessive BAFF levels have been implicated in several B-lineage malignancies (45-48), which have also been reported in the context of STK4 deficiency with or without EBV viremia (2, 5-8, 10). Our observations provide further mechanistic insights into the susceptibility of STK4-deficient patients to malignancies, although they do not allow firm conclusions about the role of EBV in this process. Nonetheless, it is tempting to speculate that STK4-deficient patients, particularly those with persistent EBV viremia, may benefit from treatment with immune checkpoint inhibitors. Using a humanized mouse model, Ma *et al.* (49) demonstrated a direct beneficial effect of PD-1/CTLA-4 blockade mediated by monoclonal antibodies against PD-1 or CTLA-4 alone, or in combination, on EBV-associated B cell lymphomas, thereby providing further evidence in support of this hypothesis. On the other hand, several research groups have reported TB reactivation or primary Mtb infections in cancer patients who received checkpoint inhibitors (50-52). Therefore, the potential benefit of the use of checkpoint inhibitors in patients with STK4 deficiency requires further investigation.

Declarations

Funding: This work was supported by a grant from the Qatar National Research Fund (Grant no. NPRP9-251-3-045) and funds from Sidra Medicine (SDR400048, SDR400013).

Conflicts of interest/Competing interests: The authors have no conflicts of interest to declare that are relevant to the content of this article.

Availability of data and material: All processed data are available in the manuscript or the supplementary materials. Raw and processed sequence read data from the PhIP-Seq experiments are available from the corresponding author on reasonable request. Raw and processed RNA-Seq data are available at the Gene Expression Omnibus (GEO), series accession number GSE166761.

Code availability: Python in-house scripts used in this study are available from the corresponding author on reasonable request.

Authors' contributions: NM conceived the study and supervised the project. AG, SB, RM, BL, MR, MA, FA, DP and KD designed and performed experiments. TK, AG, SB, WA, TH and NM analyzed and interpreted the flow cytometry, PhIP-Seq and high-throughput gene expression data as well as the RNA-Seq data. RM and BL analyzed STK4 gene and protein expression. KF and RC provided and analyzed the WGS data. MJ, DL, MK, AH and MA contributed the clinical data. AS, QZ, ECS, FA, MR and AR helped with the subject recruitment. AG, NM and SB wrote the paper.

Ethics approval: The study protocol was approved by the institutional review board (IRB) of Sidra Medicine (protocol no. 1601002512) and Weill Cornell Medicine, Qatar (protocol no. 13-00065).

Consent to participate: Written informed consent was obtained from each participant in accordance with local regulations governing human subject research.

Consent for publication: All authors have seen and approved the manuscript, which has not been accepted or published elsewhere.

Acknowledgments

The authors would like to thank the patient and his family for participating in this study. The authors also thank Stephen Elledge (Brigham and Women's Hospital, Harvard University Medical School) for kindly providing the VirScan phage library, the Integrated Genomics Core and Deep Phenotyping Services team of Sidra Medicine for their assistance with the high-throughput PCR experiments, RNA sequencing and flow cytometry; and Jessica Tamanini (Insight Editing London) for proofreading and editing the manuscript.

References

1. Tangye SG, Al-Herz W, Bousfiha A, Chatila T, Cunningham-Rundles C, Etzioni A, et al. Correction to: Human Inborn Errors of Immunity: 2019 Update on the Classification from the International Union of Immunological Societies Expert Committee. J Clin Immunol. 2020;40(1):65.

2. Nehme NT, Schmid JP, Debeurme F, Andre-Schmutz I, Lim A, Nitschke P, et al. MST1 mutations in autosomal recessive primary immunodeficiency characterized by defective naive T-cell survival. Blood. 2012;119(15):3458-68.

3. Abdollahpour H, Appaswamy G, Kotlarz D, Diestelhorst J, Beier R, Schaffer AA, et al. The phenotype of human STK4 deficiency. Blood. 2012;119(15):3450-7.

4. Schipp C, Schlutermann D, Honscheid A, Nabhani S, Holl J, Oommen PT, et al. EBV Negative Lymphoma and Autoimmune Lymphoproliferative Syndrome Like Phenotype Extend the Clinical Spectrum of Primary Immunodeficiency Caused by STK4 Deficiency. Front Immunol. 2018;9:2400.

5. Dang TS, Willet JD, Griffin HR, Morgan NV, O'Boyle G, Arkwright PD, et al. Defective Leukocyte Adhesion and Chemotaxis Contributes to Combined Immunodeficiency in Humans with Autosomal Recessive MST1 Deficiency. J Clin Immunol. 2016;36(2):117-22.

6. Sherkat R, Sabri MR, Dehghan B, Bigdelian H, Reisi N, Afsharmoghadam N, et al. EBV lymphoproliferative-associated disease and primary cardiac T-cell lymphoma in a STK4 deficient patient: A case report. Medicine (Baltimore). 2017;96(48):e8852.

7. Radwan N, El-Owaidy R, El-Sayed ZA, Abdel-Baky A, El-Haddad A, Rashad H, et al. A Case of STK4 Deficiency with Complications Evoking Mycobacterial Infection. J Clin Immunol. 2020;40(4):665-9.

8. Lum SH, Bonney D, Cheesman E, Wrignt NB, Hughes S, Wynn R. Successful Curative Therapy With Rituximab and Allogeneic Haematopoietic Stem Cell Transplantation for MALT Lymphoma Associated With STK4-Mutated CD4+ Lymphocytopenia. Pediatr Blood Cancer. 2016;63(9):1657-9.

9. Ashrafi F, Klein C, Poorpooneh M, Sherkat R, Khoshnevisan R. A case report of sinusoidal diffuse large B-cell lymphoma in a STK4 deficient patient. Medicine (Baltimore). 2020;99(9):e18601.

10. Al-Saud B, Alajlan H, Sabar H, Anwar S, Alruwaili H, Al-Hussain T, et al. STK4 Deficiency in a Patient with Immune Complex Glomerulonephritis, Salt-Losing Tubulopathy, and Castleman's-Like Disease. J Clin Immunol. 2019;39(8):823-6.

11. Sharafian S, Ziaee V, Shahrooei M, Ahadi M, Parvaneh N. A Novel STK4 Mutation Presenting with Juvenile Idiopathic Arthritis and Epidermodysplasia Verruciformis. J Clin Immunol. 2019;39(1):11-4.

12. Crequer A, Picard C, Patin E, D'Amico A, Abhyankar A, Munzer M, et al. Inherited MST1 deficiency underlies susceptibility to EV-HPV infections. PLoS One. 2012;7(8):e44010.

13. Choi J, Oh S, Lee D, Oh HJ, Park JY, Lee SB, et al. Mst1-FoxO signaling protects Naive T lymphocytes from cellular oxidative stress in mice. PLoS One. 2009;4(11):e8011.

14. Ueda Y, Kondo N, Kinashi T. MST1/2 Balance Immune Activation and Tolerance by Orchestrating Adhesion, Transcription, and Organelle Dynamics in Lymphocytes. Front Immunol. 2020;11:733.

15. Jorgensen SE, Al-Mousawi A, Assing K, Hartling U, Grosen D, Fisker N, et al. STK4 Deficiency Impairs Innate Immunity and Interferon Production Through Negative Regulation of TBK1-IRF3 Signaling. J Clin Immunol. 2020.

16. Li H, Durbin R. Fast and accurate short read alignment with Burrows-Wheeler transform. Bioinformatics. 2009;25(14):1754-60.

17. DePristo MA, Banks E, Poplin R, Garimella KV, Maguire JR, Hartl C, et al. A framework for variation discovery and genotyping using next-generation DNA sequencing data. Nat Genet. 2011;43(5):491-8.

18. Cingolani P, Platts A, Wang le L, Coon M, Nguyen T, Wang L, et al. A program for annotating and predicting the effects of single nucleotide polymorphisms, SnpEff: SNPs in the genome of Drosophila melanogaster strain w1118; iso-2; iso-3. Fly (Austin). 2012;6(2):80-92.

19. Love JM, Prosser D, Love DR, Chintakindi KP, Dalal AB, Aggarwal S. A novel glycine decarboxylase gene mutation in an Indian family with nonketotic hyperglycinemia. J Child Neurol. 2014;29(1):122-7.

20. Alsina L, Israelsson E, Altman MC, Dang KK, Ghandil P, Israel L, et al. A narrow repertoire of transcriptional modules responsive to pyogenic bacteria is impaired in patients carrying loss-of-function mutations in MYD88 or IRAK4. Nat Immunol. 2014;15(12):1134-42.

21. de Jonge HJ, Fehrmann RS, de Bont ES, Hofstra RM, Gerbens F, Kamps WA, et al. Evidence based selection of housekeeping genes. PLoS One. 2007;2(9):e898.

22. Livak KJ, Schmittgen TD. Analysis of relative gene expression data using real-time quantitative PCR and the 2(-Delta Delta C(T)) Method. Methods. 2001;25(4):402-8.

23. Dobin A, Davis CA, Schlesinger F, Drenkow J, Zaleski C, Jha S, et al. STAR: ultrafast universal RNA-seq aligner. Bioinformatics. 2013;29(1):15-21.

24. Anders S, Pyl PT, Huber W. HTSeq--a Python framework to work with high-throughput sequencing data. Bioinformatics. 2015;31(2):166-9.

641 25. Zhang Y, Parmigiani G, Johnson WE. ComBat-seq: batch effect adjustment for RNA-seq
642 count data. NAR Genom Bioinform. 2020;2(3):lqaa078.

643 26. Robinson MD, McCarthy DJ, Smyth GK. edgeR: a Bioconductor package for differential
644 expression analysis of digital gene expression data. Bioinformatics. 2010;26(1):139-40.

645 27. Li J, Ritelli M, Ma CS, Rao G, Habib T, Corvilain E, et al. Chronic mucocutaneous
646 candidiasis and connective tissue disorder in humans with impaired JNK1-dependent
647 responses to IL-17A/F and TGF-beta. Sci Immunol. 2019;4(41).

648 28. Mohan D, Wansley DL, Sie BM, Noon MS, Baer AN, Laserson U, et al. Publisher
649 Correction: PhIP-Seq characterization of serum antibodies using oligonucleotide-
650 encoded peptidomes. Nat Protoc. 2019;14(8):2596.

651 29. Xu GJ, Kula T, Xu Q, Li MZ, Vernon SD, Ndung'u T, et al. Viral immunology.
652 Comprehensive serological profiling of human populations using a synthetic human
653 virome. Science. 2015;348(6239):aaa0698.

654 30. Khan T, Rahman M, Ali FA, Huang SSY, Ata M, Zhang Q, et al. Distinct antibody
655 repertoires against endemic human coronaviruses in children and adults. JCI Insight.
656 2021;6(4).

657 31. Mina MJ, Kula T, Leng Y, Li M, de Vries RD, Knip M, et al. Measles virus infection
658 diminishes preexisting antibodies that offer protection from other pathogens. Science.
659 2019;366(6465):599-606.

660 32. Hasan MR, Rahman M, Khan T, Saeed A, Sundararaju S, Flores A, et al. Virome-wide
661 serological profiling reveals association of herpesviruses with obesity. Sci Rep.
662 2021;11(1):2562.

33. Halacli SO, Ayvaz DC, Sun-Tan C, Erman B, Uz E, Yilmaz DY, et al. STK4 (MST1) deficiency in two siblings with autoimmune cytopenias: A novel mutation. Clin Immunol. 2015;161(2):316-23.

34. Hong JJ, Amancha PK, Rogers K, Ansari AA, Villinger F. Re-evaluation of PD-1 expression by T cells as a marker for immune exhaustion during SIV infection. PLoS One. 2013;8(3):e60186.

35. Hofmeyer KA, Jeon H, Zang X. The PD-1/PD-L1 (B7-H1) pathway in chronic infection-induced cytotoxic T lymphocyte exhaustion. J Biomed Biotechnol. 2011;2011:451694.

36. Dong Y, Li X, Zhang L, Zhu Q, Chen C, Bao J, et al. CD4(+) T cell exhaustion revealed by high PD-1 and LAG-3 expression and the loss of helper T cell function in chronic hepatitis B. BMC Immunol. 2019;20(1):27.

37. Grywalska E, Smarz-Widelska I, Korona-Glowniak I, Mertowski S, Gosik K, Hymos A, et al. PD-1 and PD-L1 Expression on Circulating Lymphocytes as a Marker of Epstein-Barr Virus Reactivation-Associated Proliferative Glomerulonephritis. Int J Mol Sci. 2020;21(21).

38. Cichocki F, Grzywacz B, Miller JS. Human NK Cell Development: One Road or Many? Front Immunol. 2019;10:2078.

39. Poli A, Michel T, Theresine M, Andres E, Hentges F, Zimmer J. CD56bright natural killer (NK) cells: an important NK cell subset. Immunology. 2009;126(4):458-65.

40. Gujer C, Murer A, Muller A, Vanoaica D, Sutter K, Jacque E, et al. Plasmacytoid dendritic cells respond to Epstein-Barr virus infection with a distinct type I interferon subtype profile. Blood Adv. 2019;3(7):1129-44.

41. Moran I, Avery DT, Payne K, Lenthall H, Davies EG, Burns S, et al. B cell-intrinsic requirement for STK4 in humoral immunity in mice and human subjects. J Allergy Clin Immunol. 2019;143(6):2302-5.

42. Pollard AJ, Bijker EM. Publisher Correction: A guide to vaccinology: from basic principles to new developments. Nat Rev Immunol. 2021;21(2):129.

43. Boisson-Dupuis S, Ramirez-Alejo N, Li Z, Patin E, Rao G, Kerner G, et al. Tuberculosis and impaired IL-23-dependent IFN-gamma immunity in humans homozygous for a common TYK2 missense variant. Sci Immunol. 2018;3(30).

44. Frederico B, May JS, Efstathiou S, Stevenson PG. BAFF receptor deficiency limits gammaherpesvirus infection. J Virol. 2014;88(8):3965-75.

45. Kuo SH, Yeh PY, Chen LT, Wu MS, Lin CW, Yeh KH, et al. Overexpression of B cell-activating factor of TNF family (BAFF) is associated with Helicobacter pylori-independent growth of gastric diffuse large B-cell lymphoma with histologic evidence of MALT lymphoma. Blood. 2008;112(7):2927-34.

46. Novak AJ, Grote DM, Stenson M, Ziesmer SC, Witzig TE, Habermann TM, et al. Expression of BLyS and its receptors in B-cell non-Hodgkin lymphoma: correlation with disease activity and patient outcome. Blood. 2004;104(8):2247-53.

47. Oki Y, Georgakis GV, Migone TS, Kwak LW, Younes A. Prognostic significance of serum B-lymphocyte stimulator in Hodgkin's lymphoma. Haematologica. 2007;92(2):269-70.

48. Onda K, Iijima K, Katagiri YU, Okita H, Saito M, Shimizu T, et al. Differential effects of BAFF on B cell precursor acute lymphoblastic leukemia and Burkitt lymphoma. Int J Hematol. 2010;91(5):808-19.

49. Ma SD, Xu X, Jones R, Delecluse HJ, Zumwalde NA, Sharma A, et al. PD-1/CTLA-4 Blockade Inhibits Epstein-Barr Virus-Induced Lymphoma Growth in a Cord Blood Humanized-Mouse Model. PLoS Pathog. 2016;12(5):e1005642.

50. Inthasot V, Bruyneel M, Muylle I, Ninane V. Severe pulmonary infections complicating nivolumab treatment for lung cancer: a report of two cases. Acta Clin Belg. 2020;75(4):308-10.

51. Barber DL, Sakai S, Kudchadkar RR, Fling SP, Day TA, Vergara JA, et al. Tuberculosis following PD-1 blockade for cancer immunotherapy. Sci Transl Med. 2019;11(475).

52. Anastasopoulou A, Ziogas DC, Samarkos M, Kirkwood JM, Gogas H. Reactivation of tuberculosis in cancer patients following administration of immune checkpoint inhibitors: current evidence and clinical practice recommendations. J Immunother Cancer. 2019;7(1):239.

Figures

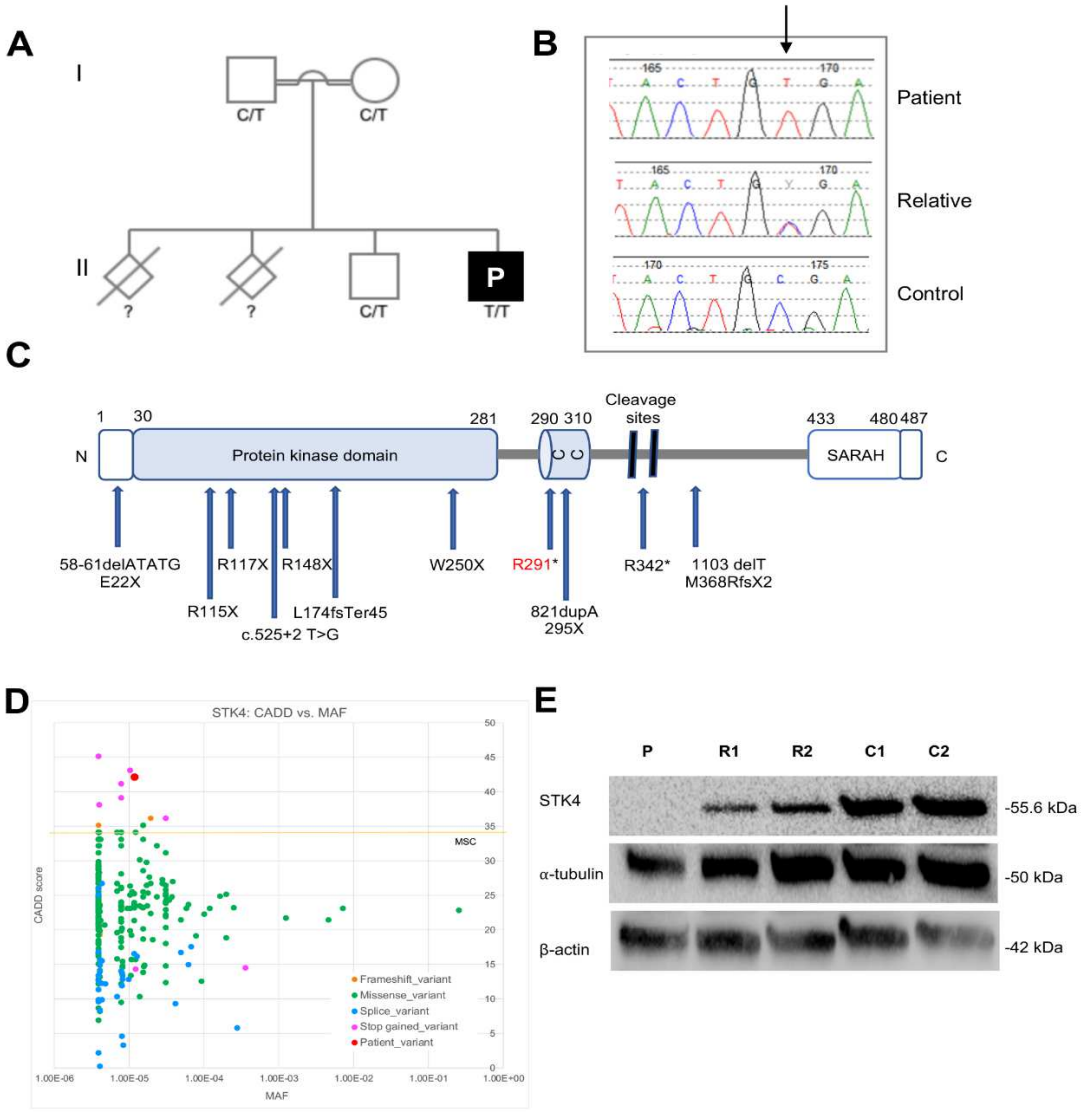

Figure 1 Identification of a homozygous *STK4* gene mutation in a patient from consanguineous parents. (**A**) Pedigree and segregation of the *STK4* gene mutation. The patient (P) is homozygous for the mutation. Question marks (?) indicate individuals whose genetic status could not be evaluated. (**B**) Electropherograms of partial sequences of *STK4* corresponding to the mutation in a healthy control (bottom), patient (up) and one of the patient's STK4$^{wt/mut}$ relatives (middle), representative for any of the three healthy family members. The reference vs. altered nucleotide position is indicated by a black arrow. (**C**) Schematic illustration of the protein encoded by the *STK4* gene, with domain boundaries and other features retrieved from the UniProtKB (www.uniprot.org) (entry Q13043). Blue arrows indicate previously reported variants (2-5, 9-12, 15, 33). The variant of the patient in the present study is indicated in red text. CC, coiled coil domain; SARAH, Sav/Rassf/Hpo domain (IPR024205). (**D**) Combined annotation-dependent depletion score (CADD) serves as a measure to predict the functional impact of the variant. Data from the gnomAD database were used to plot minor allele frequency (MAF) against the CADD score values of all known variants in *STK4* and the patient's variant. (**E**) Western blot analysis of STK4 protein expression in PBMC-derived T lymphocytes from the patient (P), two STK4$^{wt/mut}$ heterozygeous relatives (R1 and R2) and two unrelated STK4$^{wt/wt}$, healthy controls (C1 and C2); α-tubulin and β-actin antibodies were used as controls.

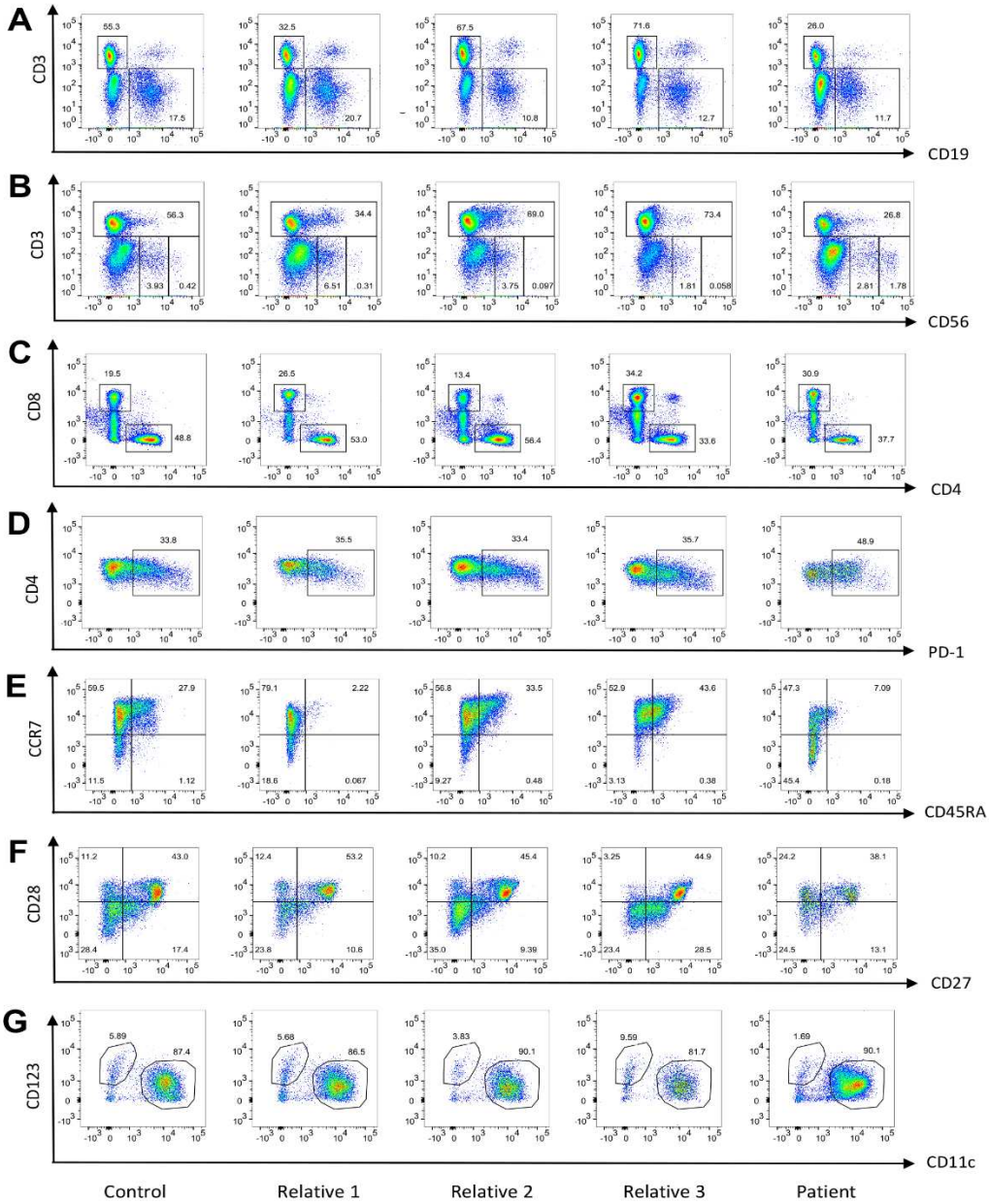

Figure 2 Leukocyte subsets in the STK4-deficient patient, his parents and sibling, and one unrelated healthy control. For all experiments, subjects are presented in the following order from left to right: Unrealted control, the patient's three relatives, and the patient. (**A**) Frequency of B ($CD3^-CD19^+$) and T lymphocytes ($CD3^+CD19^-$) among $CD45^+$ lymphocytes. (**B**) Frequency of T lymphocytes ($CD3^+$) and NK cell immunophenotyping, showing the frequency of $CD56^{bright}$ ($CD3^+CD56^{bright}$) and $CD56^{dim}$ ($CD3^+CD56^{dim}$) NK cells among $CD45^+$ lymphocytes. (**C**) Frequency of cytotoxic ($CD3^+CD8^+$) and helper ($CD3^+CD4^+$) T lymphocytes among the $CD3^+$ lymphocyte subset. (**D**) Frequency of PD-1^+ T lymphocytes ($CD4^+$PD-1^+) among the $CD4^+$ T cell subset. (**E**) Frequency of naïve ($CD45RA^+CCR7^+$), central memory ($CD45RA^-CCR7^+$), effector memory ($CD45RA^-CCR7^-$) and effector memory cells re-expressing CD45RA (T_{EMRA}) ($CD45RA^+CCR7^-$) cells among the $CD4^+$ T cell compartment. (**F**) Frequency of $CD27^+$ and $CD28^+$ T helper subsets within the $CD4^+$ compartment. (**G**) Frequency of myeloid dendritic cells (mDCs) ($CD123^-CD11c^+$) and plasmacytoid dendritic cells (pDCs) ($CD123^+CD11c^-$) among the $CD45^+$HLA-$DR^+CD3^-CD14^-CD19^-$, $CD20^-CD56^-$ dendritic cell population.

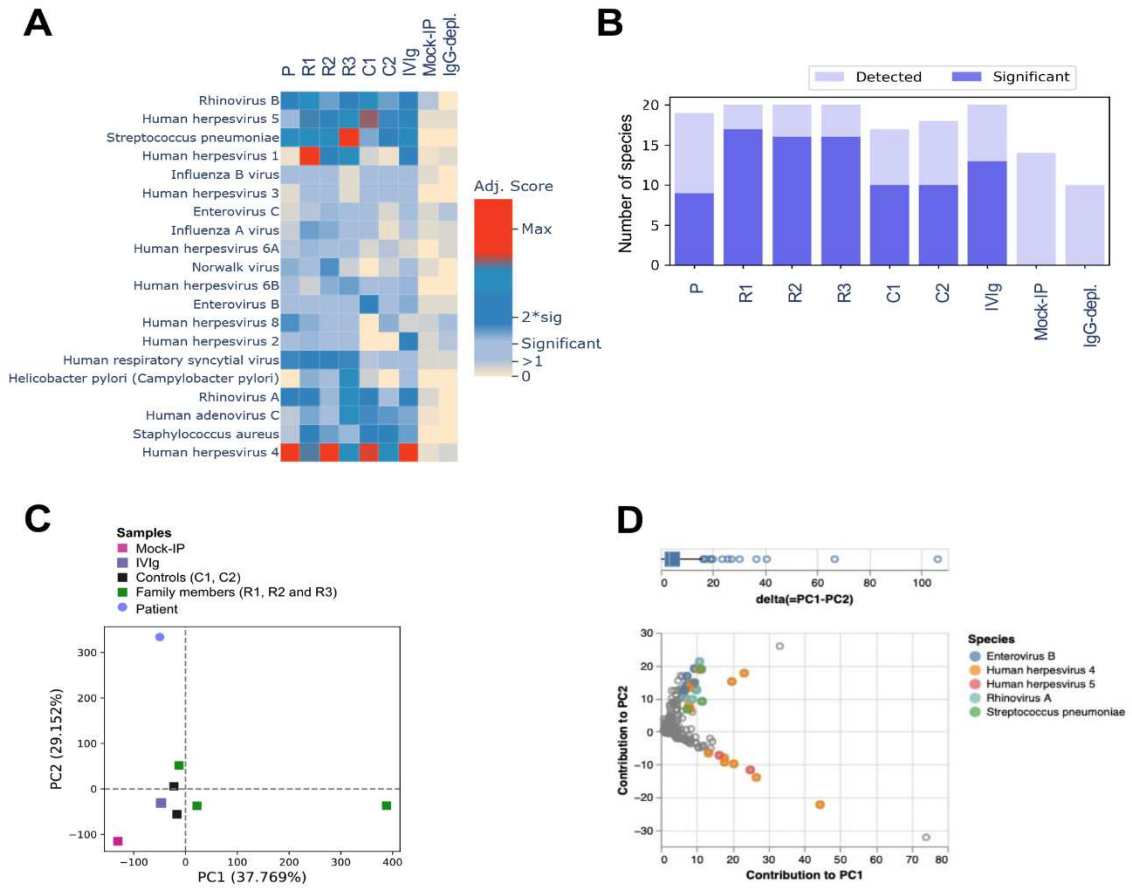

Figure 3 Microbial exposure profile and antiviral antibody repertoire in the STK4-deficient patient. (**A**) Antibody profile in the STK4$^{-/-}$ patient (P), his STK4$^{WT/-}$ family members (R1, R2 and R3) as well as two unrelated STK4$^{WT/WT}$ controls (C1 and C2). Pooled human plasma used for intravenous immunoglobulin therapy (IVIg), human IgG-depleted serum (IgG-depl.) and mock-IP samples served as additional controls. The heatmap plot shows species-specific adjusted score values, which served as a quantitative measure of the number of antibody specificities targeting a given microbial species. (**B**) Bar plot depicting, for each sample shown in (**A**), the number of species for which peptides were significantly enriched by PhIP-Seq (i.e., at least one antibody specificity was detected) (light blue) and number of species for which the adjusted virus score values passed the significance cut-off (i.e., the sample was considered seropositive for that given species) (dark blue). (**C**) Principal component analysis (PCA) of the -log$_{10}$(*P*-values) of significantly enriched peptides for each sample as shown in (**A**). The scatter plot shows the contribution of the significantly enriched peptides to principal component (PC)1 and PC2. (**D**) Scatter plot showing the contribution of enriched peptides in the patient's sample to PC1 and PC2. Peptides are color-coded by species. Peptides shown in grey correspond to species for which less than two peptides had a delta (PC1-PC2) of more than the 70th percentile (top).

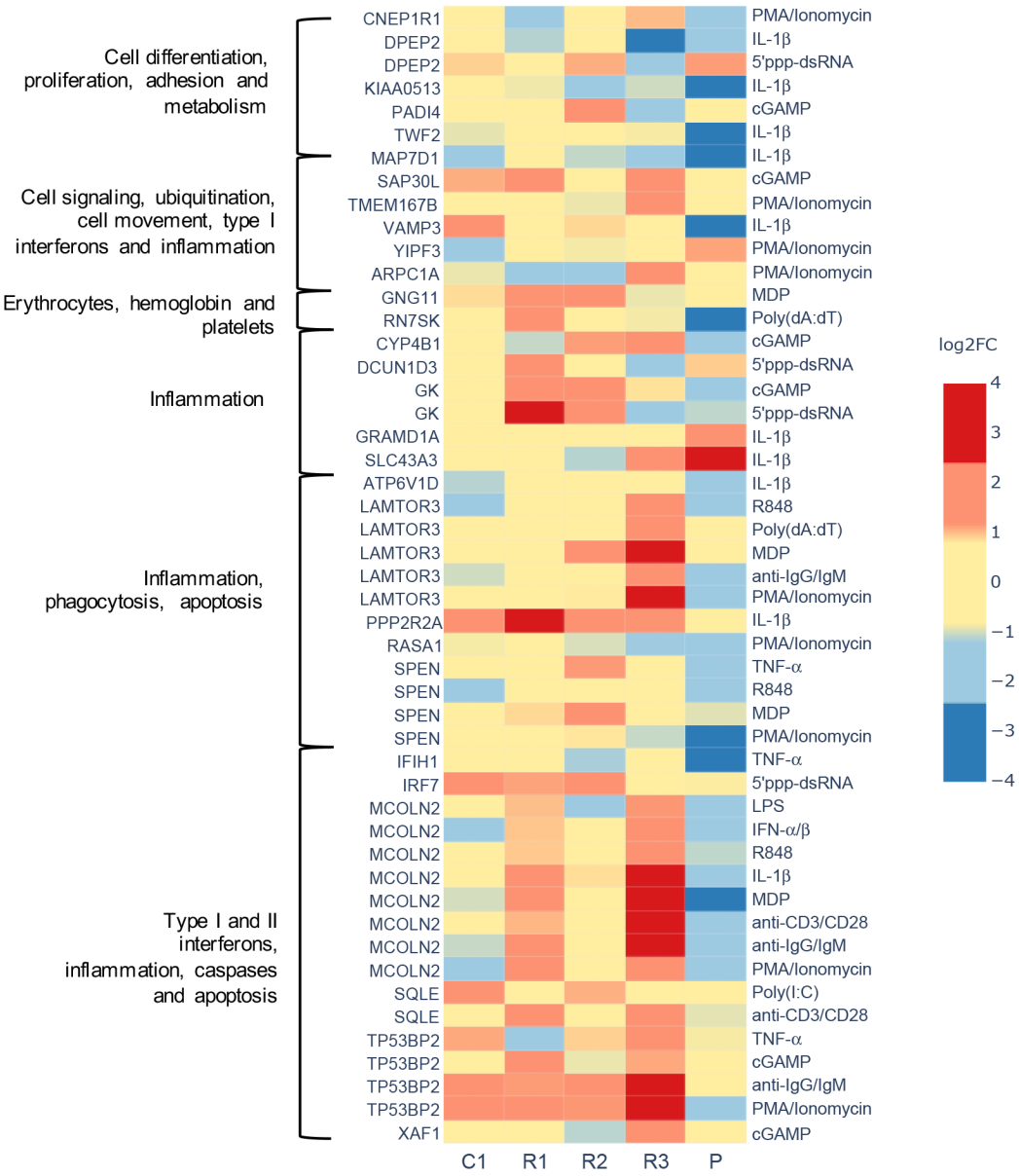

Figure 4 Unique gene expression signature in whole blood samples from the STK4-deficient patient following *in vitro* stimulation. The heatmap shows the log_2-transformed fold change values (log2FC) of the differentially expressed genes (DEGs) among the 180 target genes for which transcriptional responses in the patient's (P) whole blood samples to *in vitro* stimulation showed a variance of |log2FC| >1 compared to those of the other family members (R1, R2 and R3) and an unrelated control (C1). Gene-stimuli pairs are grouped according to the functional annotation of the gene cluster as described previously (20).

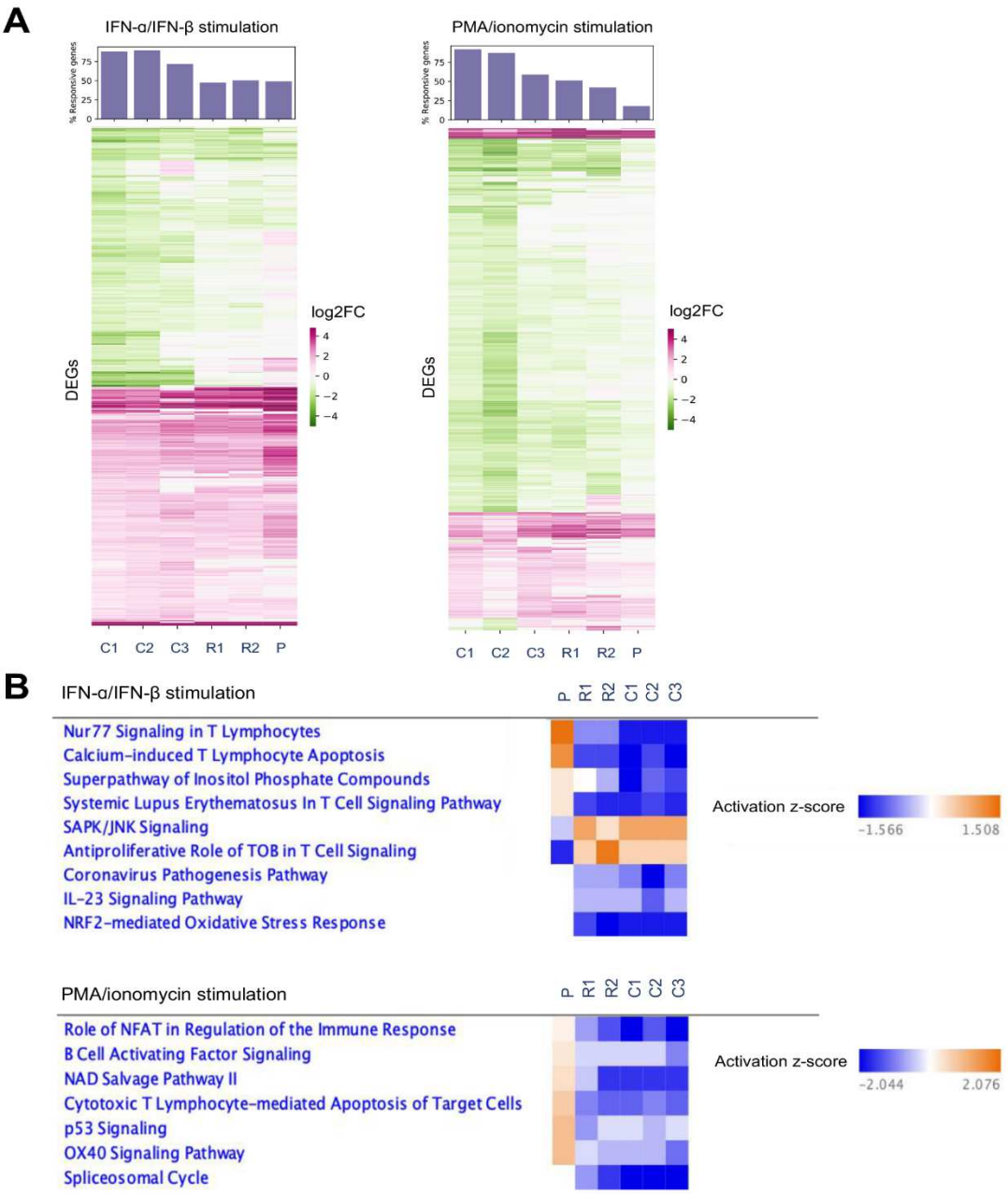

Figure 5 RNA-Seq and gene enrichment analysis of stimulated PBMCs. (A) The heatmaps show log_2-transformed fold change values (log2FC) of differentially expressed genes (DEGs) following *in vitro* stimulation of PBMCs obtained from the STK4-deficient patient (P), two of his family members (R1 and R2) and three unrelated controls (C1, C2 and C3) with either recombinant human IFN-α and IFN-β (left), or PMA and ionomycin (right). Pink indicates activated genes and green indicates repressed genes. (**B**) Heatmaps show the activation z-score values of a canonical pathway comparison analysis using the QIAGEN Ingenuity Pathway Analysis software for stimulation with recombinant human IFN-α and IFN-β (top), or PMA and ionomycin (bottom). Red indicates activated pathways and blue indicates repressed pathways.

Figures

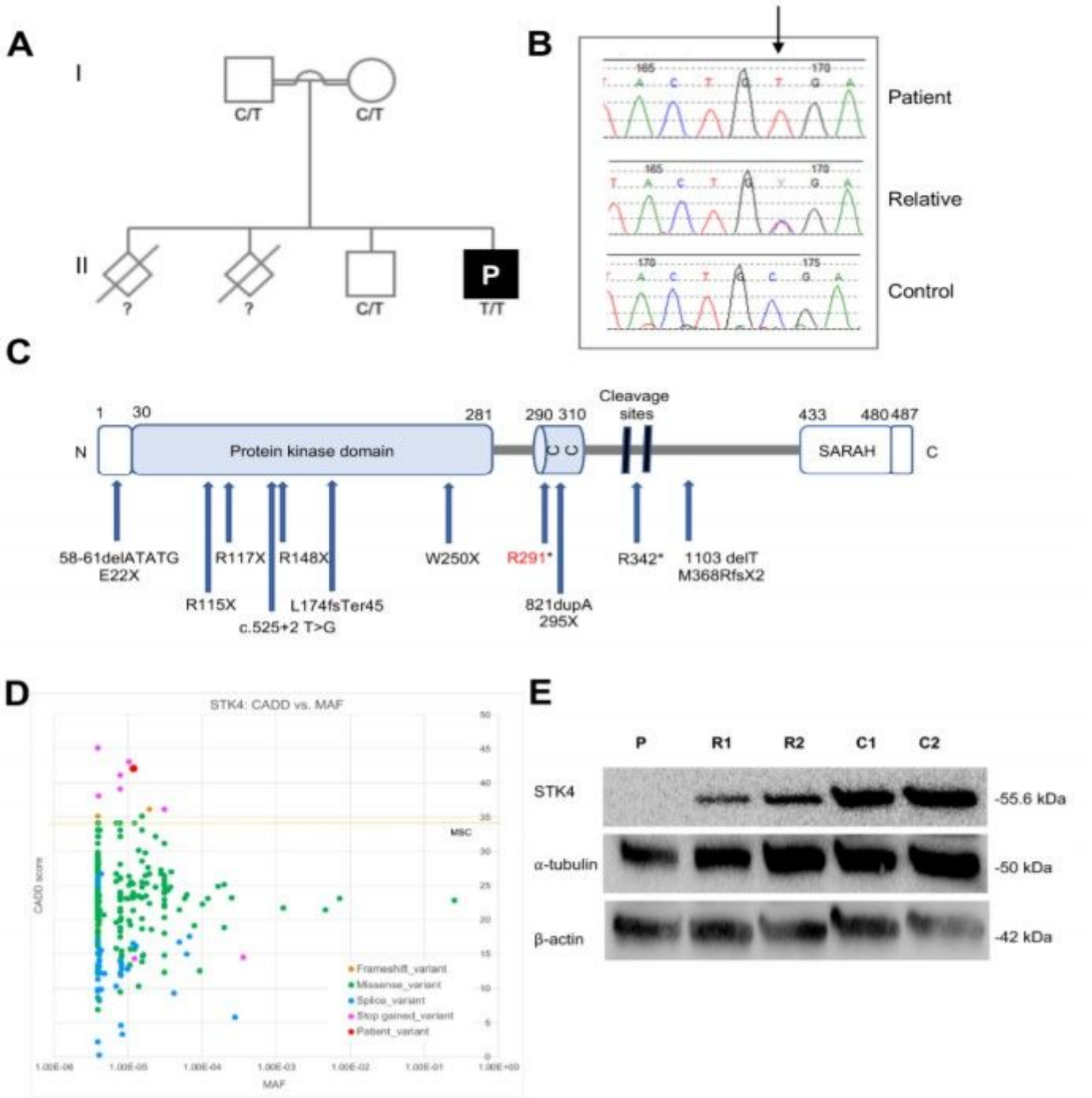

Figure 1

Identification of a homozygous STK4 gene mutation in a patient from consanguineous parents. (A) Pedigree and segregation of the STK4 gene mutation. The patient (P) is homozygous for the mutation. Question marks (?) indicate individuals whose genetic status could not be evaluated. (B) Electropherograms of partial sequences of STK4 corresponding to the mutation in a healthy control (bottom), patient (up) and one of the patient's STK4wt/mut relatives (middle), representative for any of

the three healthy family members. The reference vs. altered nucleotide position is indicated by a black arrow. (C) Schematic illustration of the protein encoded by the STK4 gene, with domain boundaries and other features retrieved from the UniProtKB (www.uniprot.org) (entry Q13043). Blue arrows indicate previously reported variants (2-5, 9-12, 15, 33). The variant of the patient in the present study is indicated in red text. CC, coiled coil domain; SARAH, Sav/Rassf/Hpo domain (IPR024205). (D) Combined annotation-dependent depletion score (CADD) serves as a measure to predict the functional impact of the variant. Data from the gnomAD database were used to plot minor allele frequency (MAF) against the CADD score values of all known variants in STK4 and the patient's variant. (E) Western blot analysis of STK4 protein expression in PBMC-derived T lymphocytes from the patient (P), two STK4wt/mut heterozygeous relatives (R1 and R2) and two unrelated STK4wt/wt , healthy controls (C1 and C2); a-tubulin and b-actin antibodies were used as controls.

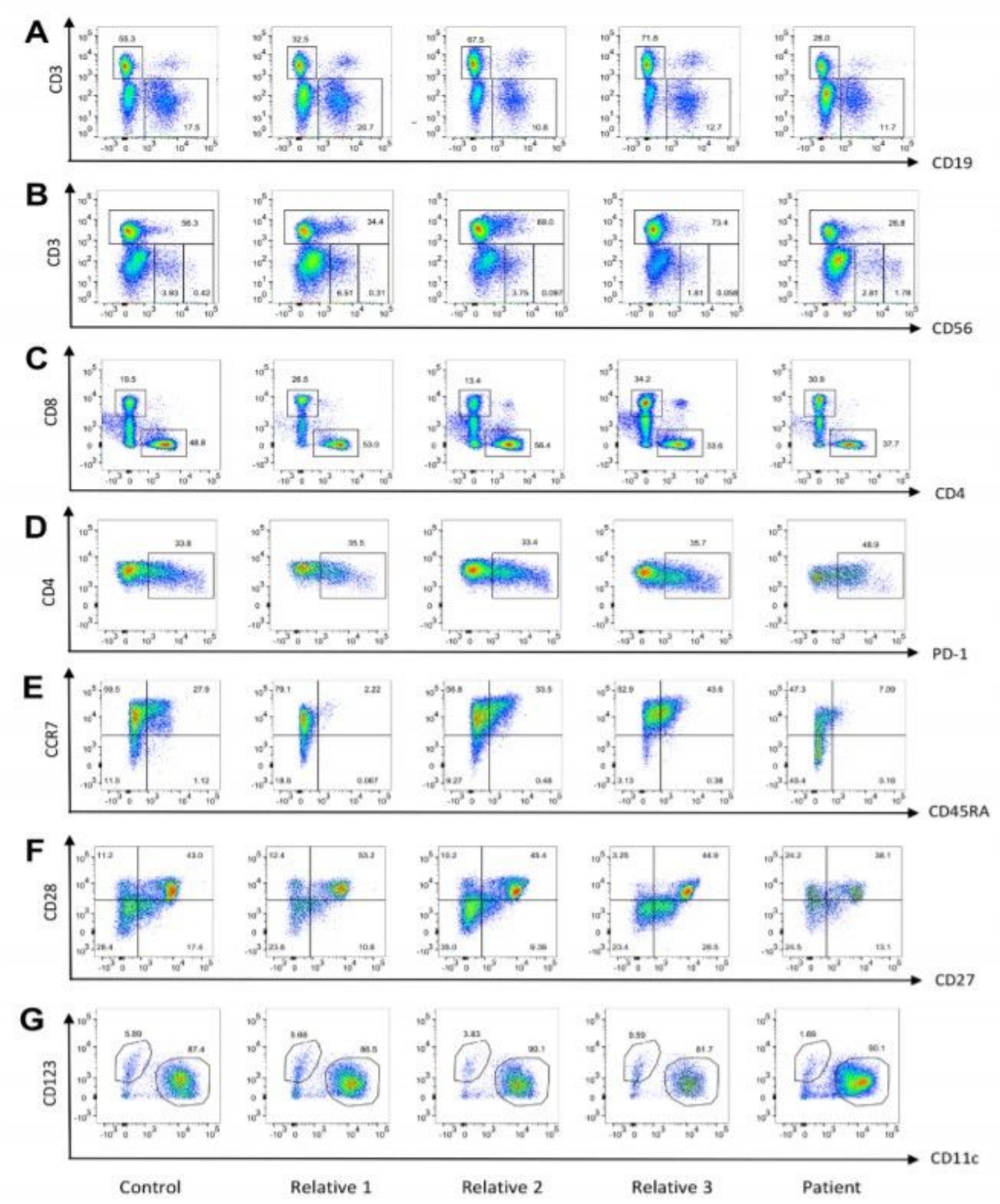

Figure 2

Leukocyte subsets in the STK4-deficient patient, his parents and sibling, and one unrelated healthy control. For all experiments, subjects are presented in the following order from left to right: Unrealted control, the patient's three relatives, and the patient. (A) Frequency of B (CD3- CD19+) and T lymphocytes (CD3+ CD19-) among CD45+ lymphocytes. (B) Frequency of T lymphocytes (CD3+) and NK cell immunophenotyping, showing the frequency of CD56bright (CD3+ CD56bright) and CD56dim (CD3+

CD56dim) NK cells among CD45+ lymphocytes. (C) Frequency of cytotoxic (CD3+ CD8+) and helper (CD3+ CD4+) T lymphocytes among the CD3+ lymphocyte subset. (D) Frequency of PD-1+ T lymphocytes (CD4+ PD-1+) among the CD4+ T cell subset. (E) Frequency of naïve (CD45RA+ CCR7+), central memory (CD45RACCR7+), effector memory (CD45RACCR7-) and effector memory cells reexpressing CD45RA (TEMRA) (CD45RA+ CCR7-) cells among the CD4+ T cell compartment. (F) Frequency of CD27+ and CD28+ T helper subsets within the CD4+ compartment. (G) Frequency of myeloid dendritic cells (mDCs) (CD123- CD11c+) and plasmacytoid dendritic cells (pDCs) (CD123+ CD11c-) among the CD45+ HLA-DR+ CD3- CD14- CD19- , CD20- CD56- dendritic cell population.

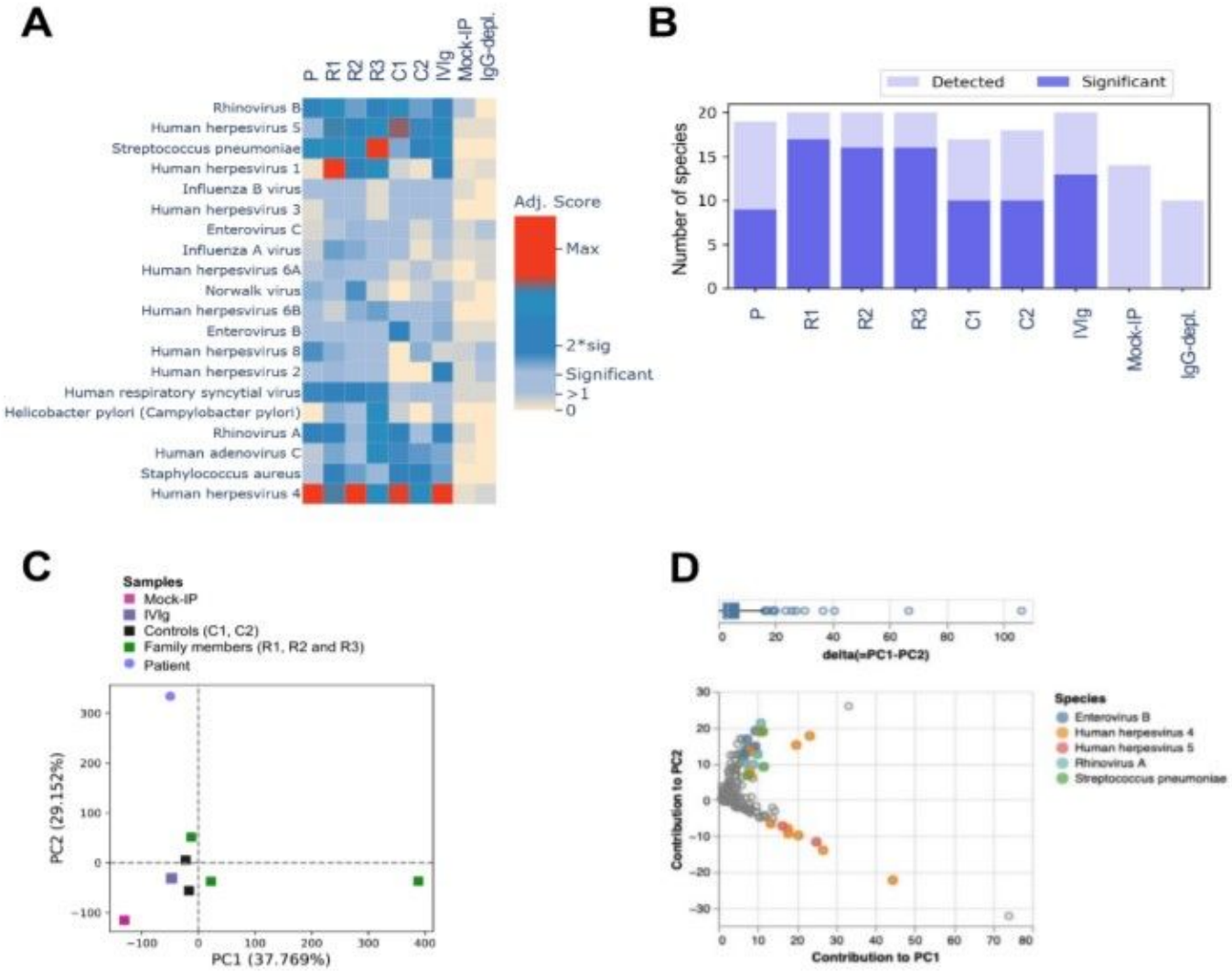

Figure 3

Microbial exposure profile and antiviral antibody repertoire in the STK4- deficient patient. (A) Antibody profile in the STK4-/- patient (P), his STK4WT/- family members (R1, R2 and R3) as well as two unrelated STK4WT/WT controls (C1 and C2). Pooled human plasma used for intravenous immunoglobulin therapy (IVIg), human IgG-depleted serum (IgG depl.) and mock-IP samples served as additional controls. The heatmap plot shows species specific adjusted score values, which served as a quantitative measure of the number of antibody specificities targeting a given microbial species. (B) Bar plot depicting, for each

sample shown in (A), the number of species for which peptides were significantly enriched by PhIP-Seq (i.e., at least one antibody specificity was detected) (light blue) and number of species for which the adjusted virus score values passed the significance cut-off (i.e., the sample was considered seropositive for that given species) (dark blue). (C) Principal component analysis (PCA) of the -log10(P-values) of significantly enriched peptides for each sample as shown in (A). The scatter plot shows the contribution of the significantly enriched peptides to principal component (PC)1 and PC2. (D) Scatter plot showing the contribution of enriched peptides in the patient's sample to PC1 and PC2. Peptides are color-coded by species. Peptides shown in grey correspond to species for which less than two peptides had a delta (PC1-PC2) of more than the 70th percentile (top).

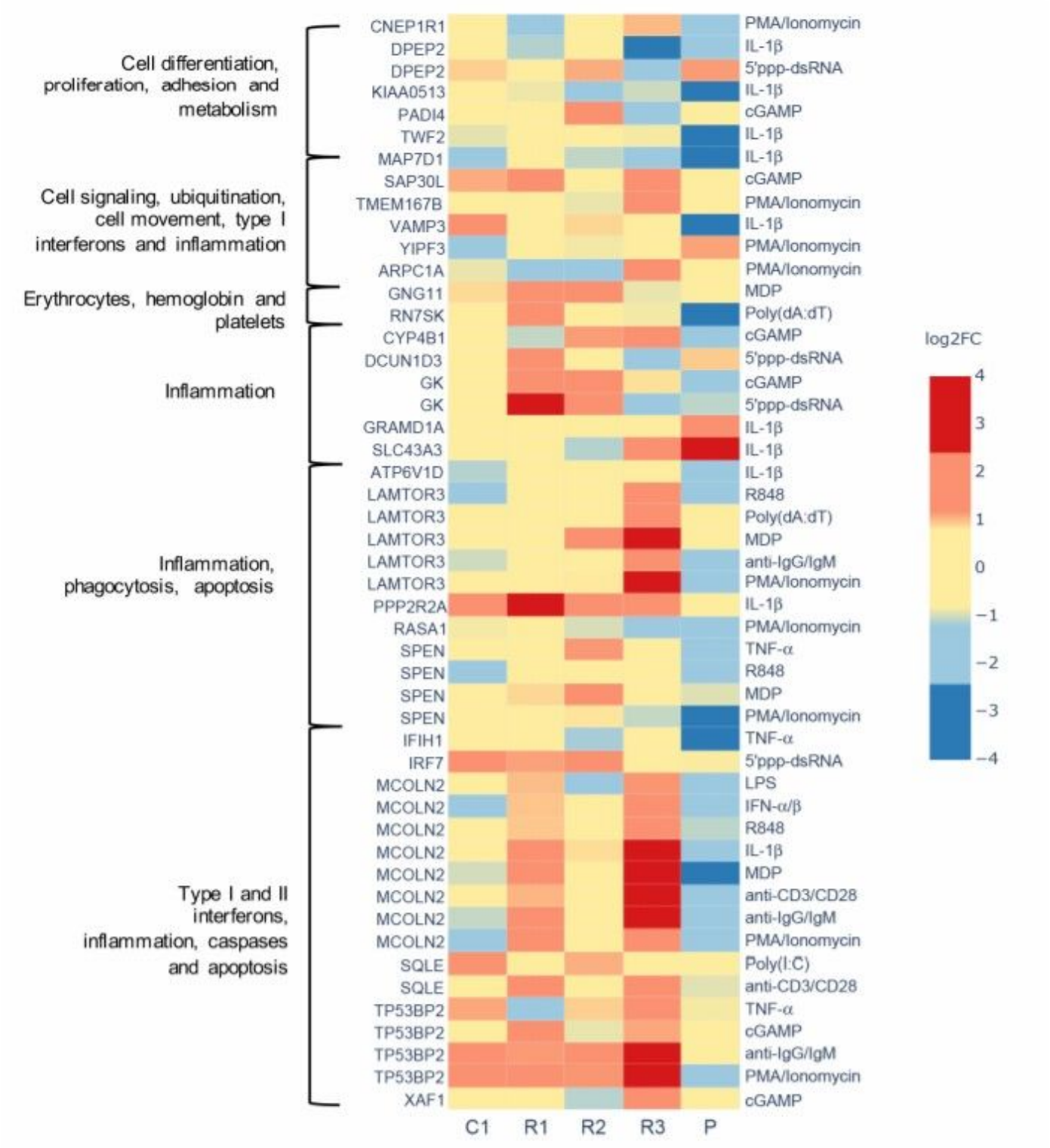

Figure 4

Unique gene expression signature in whole blood samples from the STK4-deficient patient following in vitro stimulation. The heatmap shows the log2- transformed fold change values (log2FC) of the differentially expressed genes (DEGs) among the 180 target genes for which transcriptional responses in the patient's (P) whole blood samples to in vitro stimulation showed a variance of |log2FC| >1 compared

to those of the other family members (R1, R2 and R3) and an unrelated control (C1). Gene-stimuli pairs are grouped according to the functional annotation of the gene cluster as described previously (20).

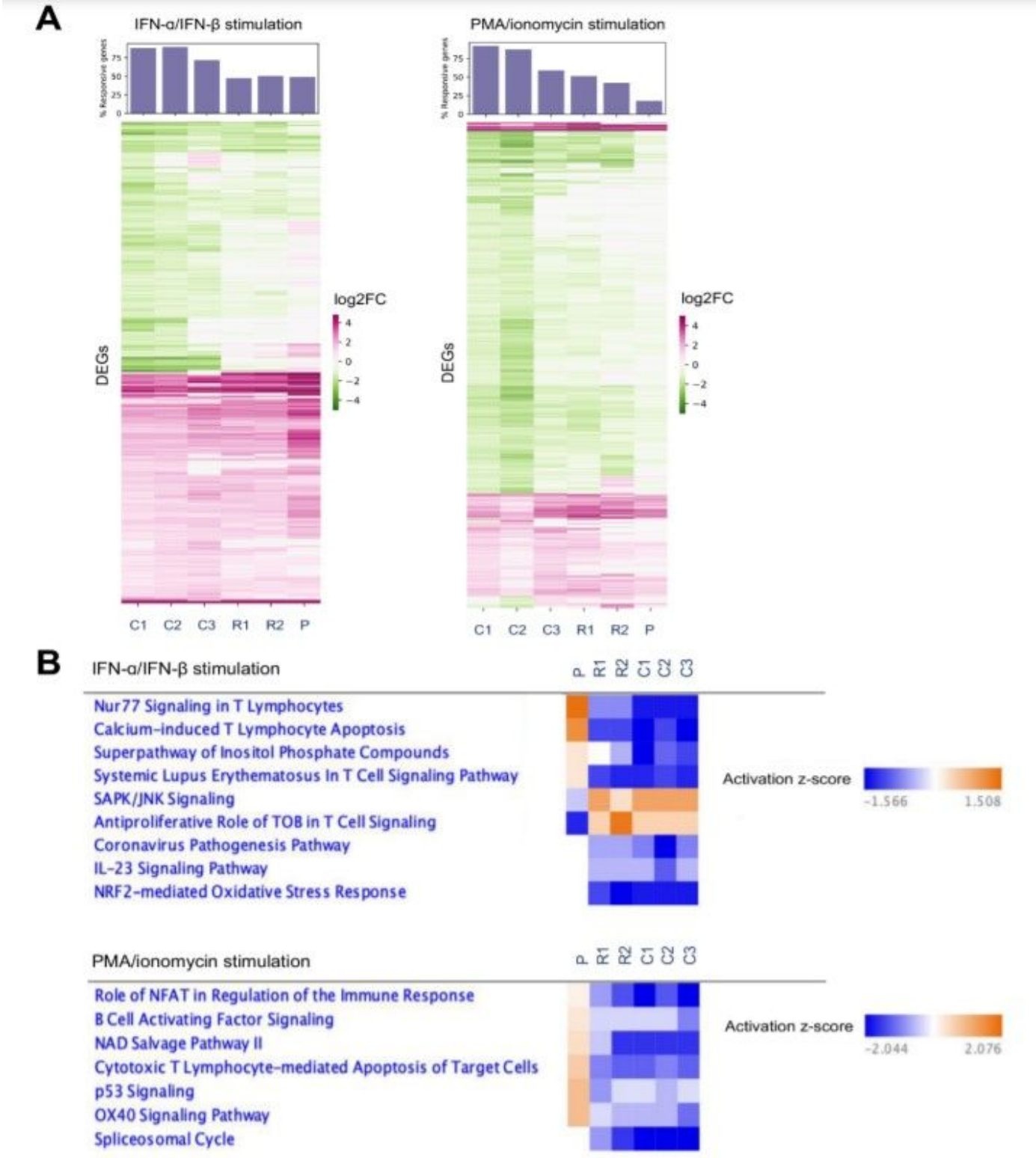

Figure 5

RNA-Seq and gene enrichment analysis of stimulated PBMCs. (A) The heatmaps show log2-transformed fold change values (log2FC) of differentially expressed genes (DEGs) following in vitro stimulation of PBMCs obtained from the STK4-deficient patient (P), two of his family members (R1 and R2) and three

unrelated controls (C1, C2 and C3) with either recombinant human IFN-a and IFN-b (left), or PMA and ionomycin (right). Pink indicates activated genes and green indicates repressed genes. (B) Heatmaps show the activation z score values of a canonical pathway comparison analysis using the QIAGEN Ingenuity Pathway Analysis software for stimulation with recombinant human IFN-a and IFN-b (top), or PMA and ionomycin (bottom). Red indicates activated pathways and blue indicates repressed pathways.

Supplementary Files

This is a list of supplementary files associated with this preprint. Click to download.

- STK4SupplementalTablesS3andS42021Mar14.xlsx
- SupplementalMaterialsSTK42021March14final.pdf